The Canadian Mineralogist
Vol. 35, pp. 95-104 (1997)

THE INCORPORATION OF ACTINIDES IN MONAZITE AND XENOTIME FROM PLACER DEPOSITS IN WESTERN AUSTRALIA

BOB VAN EMDEN

Research Centre for Advanced Mineral and Materials Processing, Department, of Chemistry, University of Western Australia, Nedlands, W.A., 6907, Australia

MIKE R. THORNBER

Research Centre for Advanced Mineral and Materials Processing, CSIRO, Division of Minerals, Waterford, W.A., 6102, Australia

JIM GRAHAM AND FRANK J. LINCOLN[1]

Research Centre for Advanced Mineral and Materials Processing, Department, of Chemistry, University of Western Australia, Nedlands, W.A., 6907, Australia

ABSTRACT

The composition of several samples of monazite-(Ce) and xenotime from placer deposits in Western Australia has been determined from the electron-microprobe analysis of many individual grains of mineral sand. A regression analysis of the results was used to identify the mechanisms of incorporation of the actinides Th and U in each mineral. Both of the substitution mechanisms $(Th,U)^{4+} + Ca^{2+} = 2REE^{3+}$ and $(Th,U)^{4+} + Si^{4+} = REE^{3+} + P^{5+}$ occur together in each of the monazite and xenotime samples. The incorporation of the actinides in monazite can, in general, be described by an approximately equal contribution of both the above-mechanisms. The incorporation of the actinides in xenotime, albeit less extensive than in monazite, can be largely accounted for by the second mechanism. The relative role of each mechanism of substitution in the two minerals is explained in terms of the size restrictions inherent in their structures. Many mineral grains exhibit combined levels of Ca and Si in excess of those expected as a result of the incorporation of Th and U. Additional mechanisms of substitution seem to be involved.

Keywords: monazite-(Ce), xenotime, actinides, incorporation, mechanisms, composition, electron-microprobe analysis, statisitical analysis, mineral sand, Western Australia.

SOMMAIRE

Nous avons déterminé la composition de plusieurs échantillons de monazite-(Ce) et de xénotime provenant de dépôts alluvionnaires en l'Australie occidentale au moyen d'analyses à la microsonde électronique. Une analyse statistique des résultats par régression a permis d'en déduire les mécanismes d'incorporation des actinides Th et U dans chaque minéral. Deux mécanismes importants, $(Th,U)^{4+} + Ca^{2+} = 2REE^{3+}$ et $(Th,U)^{4+} + Si^{4+} = REE^{3+} + P^{5+}$, seraient ensemble responsables de la présence de Th et U dans les deux minéraux. Dans la monazite, leur contribution semble à peu près égale, tandis que dans le xénotime, les actinides sont incorporés à un niveau moindre, et surtout selon le deuxième mécanisme. L'importance relative des deux mécanismes d'incorporation dans les deux minéraux dépendrait des contraintes géométriques dictées par les deux structures. Plusieurs des grains font preuve d'une teneur plus élevée en Ca + Si que celle qu'on prédit selon la teneur en Th + U. D'autres mécanismes de substitution semblent impliqués.

(Traduit par la Rédaction)

Mots-clés: monazite-(Ce), xénotime, actinides, incorporation, mécanismes, composition, données de microsonde électronique, analyse statistique, sable minéral, Australie occidentale.

[1] To whom all correspondence should be addressed. *E-mail address*: fjl@chem.uwa.edu.au.

INTRODUCTION

The rare-earth-element (*REE*) minerals monazite and xenotime are found in small amounts (generally less than 2%) in heavy-mineral concentrates obtained from placer deposits. Western Australia has large resources of both these minerals and an extensive ilmenite – titanium mineral-sand industry. The presence of the radioactive elements Th and U within these mineral samples (monazite in particular) has in recent years restricted their sale overseas (Satterthwaite 1994). A better understanding of the way in which these elements are held in their respective structures may lead to the development of more efficient methods of separating the *REE* from Th and U in the processing of the minerals to the *REE* oxides. A study of this type may also assist in deciding whether monazite and synthetic analogues should be further considered as hosts for the storage of high-level radioactive waste (McCarthy *et al.* 1978, Boatner & Sales 1988). Two major charge-balancing mechanisms of incorporation of Th and U in monazite have been proposed (Gramaccioli & Segalstad 1978)

$$(Th, U)^{4+} + Ca^{2+} = 2REE^{3+} \quad (1)$$

$$(Th, U)^{4+} + Si^{4+} = REE^{3+} + P^{5+} \quad (2)$$

The above mechanisms have been proposed purely on the basis that all four of the substituent elements Ca, Si, Th and U have been found to be present (at approximately the same levels) in monazite samples characterized by electron-microprobe analysis (EMPA). Most investigators [Mannucci *et al.* (1986) and Demartin *et al.* (1991b), for example] report substituent levels that may be charge-balanced by the above mechanisms, each to a differing extent. Kamineni *et al.* (1991) and Casillas *et al.* (1995), among others, however, have recorded levels of Ca and Si in monazite that differ significantly from the level necessary for the charge balance of the Th and U present. A more comprehensive analysis of the composition of monazite samples from a variety of source rocks is necessary to confirm the existence, and to ascertain the relative significance, of each mechanism of substitution in monazite.

Although several studies of the composition of xenotime have been conducted using electron-microprobe analysis (Åmli 1975, Demartin *et al.* 1991a, Petersen & Gault 1993), discussion of the incorporation of actinides has been limited. This is probably due to the low levels (commonly below limits of detection) of the actinides Th and U in xenotime samples. Yet, Jefford (1962) and Demartin *et al.* (1991a), for example, have found a small but significant amount of these actinides in xenotime.

In this paper, we propose that the incorporation of non-essential structural constituents (nESC) such as Th and U into the *REE*-bearing accessory minerals monazite and xenotime is controlled by the size restrictions in each of the structures. Certainly, the melt composition and temperature of crystallization will exert a strong influence over the level of nESC in the resultant accessory mineral (Wark & Miller 1993), but the selection of an appropriate counter-balancing ion (*i.e.*, Ca^{2+} or Si^{4+}) should be determined by the size restraints imposed by each mineral's structure. To test this, we have determined the correlations among the levels of Th, U, Ca and Si of a large number of monazite and xenotime grains derived from a variety of source rocks. Owing to the nature of the samples, it is not possible to relate the chemical compositions of the minerals to the melts from which they formed (Montel 1993), and thus no insight regarding the geochemical aspects of the genesis of monazite or xenotime can be presented.

EXPERIMENTAL

Description of the samples

The chosen samples consisted of concentrates of monazite and xenotime obtained from a number of heavy-mineral-sand producers in Western Australia. The samples derive from several fossil strand lines separated by up to 300 km and are products of weathering of parent Archean granites and gneisses from the western margin of the Yilgarn Block (Baxter 1990). Each sample analyzed was nominally a single-mineral concentrate obtained from a particular mineral-sand producer after several stages of magnetic and electrostatic separation.

Subsamples of monazite and xenotime concentrate from each producer were mounted in epoxy resin and diamond polished for examination by optical microscopy, scanning electron microscopy (SEM) and EMPA. Grain-counting techniques using SEM in combination with energy-dispersion spectrometry (EDS) showed that the monazite concentrates contain more than 95% monazite-(Ce), the remainder consisting of zircon and minor amounts of quartz and ilmenite. The xenotime concentrates typically contained 50% xenotime, 30% zircon and minor amounts of other heavy minerals. The monazite and xenotime grains are generally ellipsoidal and range in size from 50 to 300 μm.

Methods of analysis

A Cameca SX-50 electron microprobe with three independent wavelength-dispersion spectrometers and one energy-dispersion spectrometer was used for the quantitative analysis of individual grains. Excitation voltages of 15 kV and 20 kV and a beam current of 40 nA were used in the analysis of the monazite and xenotime samples, respectively. Four calcium aluminosilicate glasses, each containing precisely known amounts of three or four *REE* (Drake & Weill 1972), were used for calibration. Metallic yttrium was used to evaluate the level of Y in xenotime. The detection limits

were 0.16 wt% oxide for the *REE*, 0.06 wt% for Y and P, 0.17 wt% for Th and U, and 0.02 wt% for Ca and Si.

To determine the elements present, a wavelength-dispersion spectral scan was conducted on several grains of monazite and xenotime. These scans were used to determine the peak and background positions of each element and to identify overlapping peaks.

As recommended by Roeder (1985) for the EMPA of *REE* minerals (using wavelength-dispersion spectrometry), the levels of the *REE* were determined using the $L\alpha_1$ lines, with the exception of Pr (in monazite) and Ho (in xenotime), for which the overlap-free $L\beta_1$ lines were used. Overlap-correction factors for Sm and Gd in monazite, and Tm and Lu in xenotime, were determined from direct measurement of appropriate individual *REE* oxy-phosphate standards of general formula $REEP_5O_{14}$. The raw data were corrected for matrix effects using the MAGIC program based on Colby (1968).

Each composition was determined close to the center of an individual grain. Although irregular elemental zoning was noticed in occasional grains, most were found to be homogeneous. One hundred individual analyses of 100 different grains were used in the determination of the mean composition of each subsample of the five samples of monazite and three of xenotime.

Infrared spectra were recorded with a Bruker IFS66 infrared reflectance spectrometer to establish the presence or absence of OH. These spectra were recorded in the range 700 – 4000 cm^{-1} at room temperature.

Results and Discussion

The composition of monazite

Considerable variation in levels of individual elements was found among grains of the same concentrate. There was a wide spread in the compositions of grains from individual producers, of the same order as that found between producers. For this reason, the results from each concentrate sample were combined to give the results shown in Table 1. The full EMPA data-set can be obtained from the Depository of Unpublished Data, CISTI, National Research Council, Ottawa, Canada K1A 0S2. The spread suggests that the grains are from different sources, which helps to define a wider range of possible mechanisms of substitution. The average and range of compositions of each of the 14 elements analyzed for in this study compare well with those of monazite samples from granites and pegmatites (Jefferies 1985, Mannucci *et al.* 1986, Demartin *et al.* 1991b). This is to be expected, since the monazite grains were obtained from placer deposits that were formed from the weathering and erosion of felsic igneous rocks, such as granites (Baxter 1990).

Cerium is the dominant *REE*, whereas Th largely determines the actinide level of each grain of monazite. The level of Th within individual grains of monazite varies considerably, ranging from 1.2 to 21.9 wt.% ThO_2. These monazite grains also show considerable variation in levels of Ca and Si (Table 1), suggesting that they do provide a suitably diverse database from which to study how differing levels of Th are held within monazite.

The average total wt% oxide for each grain is close to 100%, indicating that all elements of significance have been considered. Low totals were often obtained for one particular mineral concentrate, and are attributed to a high porosity in these grains. The atomic sum of tetrahedrally coordinated P and Si is close to 1 atom per formula unit (*apfu*), whereas the cationic elements total only 0.946 *apfu*. This low value may be skewed, since in many cases the concentrations of Dy and Er were found to be below the detection limit and thus were not added into the averaging process.

The composition of xenotime

Little difference in mean composition was found among each of the three concentrates of xenotime in comparison to the range in element concentrations among individual grains. The mean compositions from all three producers were combined to give the results shown in Table 2. The full EMPA data-set is available from the Depository of Unpublished Data.

The mean levels of elements in the xenotime concentrates compare well with those found in xenotime samples by other investigators (Åmli 1975, Demartin *et al.* 1991a, Petersen & Gault 1993, among others). The mean level of U in the xenotime grains is greater than that found in the monazite, but the level of Th is much

TABLE 1. AVERAGE RESULTS OF ALL MONAZITE ANALYSES*

	Range (wt%)	Mean (wt%)			Atomic Proportion#	
		Mean	Std		Mean	Std
La_2O_3	8.9 - 21.0	14.53	2.13	La	0.207	0.030
Ce_2O_3	21.7 - 35.0	28.52	2.17	Ce	0.403	0.030
Pr_2O_3	1.8 - 3.2	2.53	0.26	Pr	0.036	0.003
Nd_2O_3	4.8 - 12.7	8.85	1.25	Nd	0.122	0.017
Sm_2O_3	0.36 - 2.89	1.53	0.45	Sm	0.020	0.006
Gd_2O_3	<0.16† - 2.71	0.88	0.51	Gd	0.011	0.006
Dy_2O_3	<0.16† - 1.28	0.26	0.30	Dy	0.003	0.004
Er_2O_3	<0.16† - 0.45	0.02	0.08	Er	0.000	0.001
Y_2O_3	<0.06† - 6.25	1.19	0.66	Y	0.024	0.022
ThO_2	1.2 - 21.9	8.79	0.08	Th	0.077	0.031
UO_2	<0.17† - 0.75	0.08	0.23	U	0.001	0.002
CaO	0.12 - 2.50	0.98	1.10	Ca	0.041	0.019
SiO_2	0.12 - 4.01	1.09	0.66	Si	0.042	0.026
P_2O_5	25.1 - 32.6	30.33	1.24	P	0.991	0.031
Total	92.5 - 103.1	99.58	2.10	**Total**	1.978	0.007

Notes : Std = Standard deviation.
Analyses that have levels below the detection limit were counted as having 0 wt% in the determination of the mean.
* Total of 500 analyses.
\# Calculated on the basis of 4 oxygen atoms.
† Indicates values that are below the detection limit.

TABLE 2. AVERAGE RESULTS OF ALL XENOTIME ANALYSES*

	Range (wt%)	Mean (wt%)			Atomic Proportion#	
		Mean	Std		Mean	Std
Y_2O_3	40.2 - 53.2	46.82	1.91	Y	0.825	0.022
Sm_2O_3	<0.16† - 1.82	0.47	0.22	Sm	0.005	0.002
Gd_2O_3	<0.16† - 4.56	1.91	0.59	Gd	0.021	0.007
Dy_2O_3	2.4 - 7.5	5.11	0.72	Dy	0.054	0.008
Ho_2O_3	<0.16† - 1.59	1.17	0.16	Ho	0.012	0.002
Er_2O_3	2.5 - 6.6	4.63	0.49	Er	0.048	0.005
Tm_2O_3	<0.16† - 0.70	0.70	0.14	Tm	0.007	0.001
Yb_2O_3	1.4 - 11.4	4.56	1.22	Yb	0.046	0.013
Lu_2O_3	<0.16† - 1.95	0.54	0.24	Lu	0.005	0.002
ThO_2	<0.17† - 8.44	0.46	0.68	Th	0.003	0.005
UO_2	<0.17† - 5.82	0.57	0.86	U	0.004	0.006
CaO	<0.02† - 0.54	0.06	0.06	Ca	0.002	0.002
SiO_2	<0.02† - 1.98	0.38	0.26	Si	0.013	0.009
P_2O_5	29.7 - 36.4	34.55	0.73	P	0.969	0.008
Total	96.0 - 105.2	101.93	1.17	**Total**	2.014	0.005

Notes : Std = Standard deviation.
Analyses that have levels below the detection limit were counted as having 0 wt% in the determination of the mean.
* Total of 300 analyses.
\# Calculated on the basis of 4 oxygen atoms.
† Indicates values that are below the detection limit.

lower (*cf.* Tables 1, 2). Different structural controls, presumably related to the size of ions, exist in these two minerals.

Totals near 100 wt% oxide for all xenotime samples suggest that all elements of significance have been determined. Both the sum of the tetrahedrally coordinated elements, P and Si (mean 0.983 *apfu*), and that of the large cationic elements (mean 1.034 *apfu*) are close to the expected value of 1 for xenotime, ideally (*HREE*)PO_4.

There is a rather wide range of totals for xenotime (96.0 – 105.2%); the high values probably are due to errors in the absorption corrections resulting from the use of a metal standard for Y, which would explain why the mean sum of large cationic elements is greater than 1. Low totals were commonly obtained for one particular mineral concentrate, and are attributed to a higher porosity in these grains.

Modes of incorporation in monazite

The incorporation of actinides in monazite is dominated by Th, with only a minor contribution from U, as indicated by the mean values in Table 1. The presence of both Ca and Si in similar atomic proportions to Th suggests that both of these elements are associated with the substitution of Th into the structure, and that both mechanisms (1) and (2) occur to maintain charge balance.

The plots of atomic proportion of Ca *versus* Th + U and Si *versus* Th + U for all individual compositions are shown in Figures 1a and b, respectively. They show that, in general, neither mechanism of substitution alone adequately explains the incorporation of Th and U in monazite. The variation in levels of Th and U among grains is best described by a combination of both mechanisms, as shown in Figure 1c. This is shown statistically by a comparison of correlation coefficients. Those for Ca and Si considered separately as a function of Th + U give +0.36 and +0.74, respectively; the correlation coefficient of Ca + Si with Th + U for all monazite compositions is 0.93. This improvement was expected, since neither mechanism of substitution is restricted by the cation-radius limitations imposed by the structure. Mechanism (1) involves the replacement of two atoms of *REE* with substituent cations (Ca and Th) of average effective ionic radius ($\bar{r}$) close to the radius of Sm [$\bar{r}$($^{IX}Ca^{2+}$,$^{IX}Th^{4+}$): 1.135 Å, $^{IX}Sm^{3+}$ 1.132 Å: Shannon 1976], which is freely able to be incorporated in monazite. In addition, brabantite, (Th,Ca)PO_4 (Rose 1980), is known to adopt the monazite structure. The elements Th and Si involved in mechanism (2) can combine to form huttonite, $ThSiO_4$, also with the monazite structure (Taylor & Ewing 1978).

A strong negative correlation (correlation coefficient: -0.95) was found between the atomic proportion of P and Si for all monazite compositions (Fig. 2). This relationship justifies the hypothesis that Si replaces P where it is incorporated together with Th into monazite. The magnitude of the slope of the line of best fit is significantly less than expected for a 1:1 Si-for-P substitution (Si/P slope = -0.82). This finding suggests that decreasing levels of P are insufficiently balanced by increasing levels of the substituent Si, giving rise to a small net negative charge. Although no mention of a correlation between levels of P and Si in monazite has been made previously, Jefferies (1985) also found a decrease in the level of P that was insufficiently balanced by an increase in Si. The charge imbalance resulting from this is largely compensated by the greater increase of Th + U relative to Ca + Si [(Ca + Si)/(Th + U) slope = +0.84] shown in Figure 1c.

As indicated by the low level of U in comparison to Th in the samples analyzed (Table 1), the incorporation of U^{4+} into the monazite structure is less strongly favored than Th^{4+}. This has been commonly observed for all monazite samples, especially those of granitic origin (*e.g.*, Murata *et al.* 1958), although there exist several samples where U makes a significant contribution to the total actinide content (Gramaccioli & Segalstad 1978, Demartin *et al.* 1991b). Partial correlation coefficients for Ca and Si with U (with intercorrelations with Th removed) of +0.45 and -0.34, respectively, for all grains with greater than the detection level of U, suggest that the incorporation of U in monazite occurs *via* mechanism (1) only and not by mechanism (2). Data taken from the literature [Mannucci *et al.* (1986) for example] confirm this hypothesis; where high levels of U are found to be present, there is always sufficient Ca present for charge balance (and, in general, not enough

Si). The incorporation of U in monazite by this mechanism seems to reflect atomic radii [$\bar{r}(^{IX}Ca^{2+}, ^{IX}U^{4+}) = 1.115$ Å, r of the "monazite forming" $^{IX}Gd^{3+} = 1.107$ Å)]. In addition $(Ca,U)PO_4$ crystallizes with the monazite structure-type (Muto *et al.* 1959), whereas coffinite $USiO_4$ adopts the more closely packed zircon structure-type (Fuchs & Gebert 1958), as do the *HREE* phosphates (Ni *et al.* 1995).

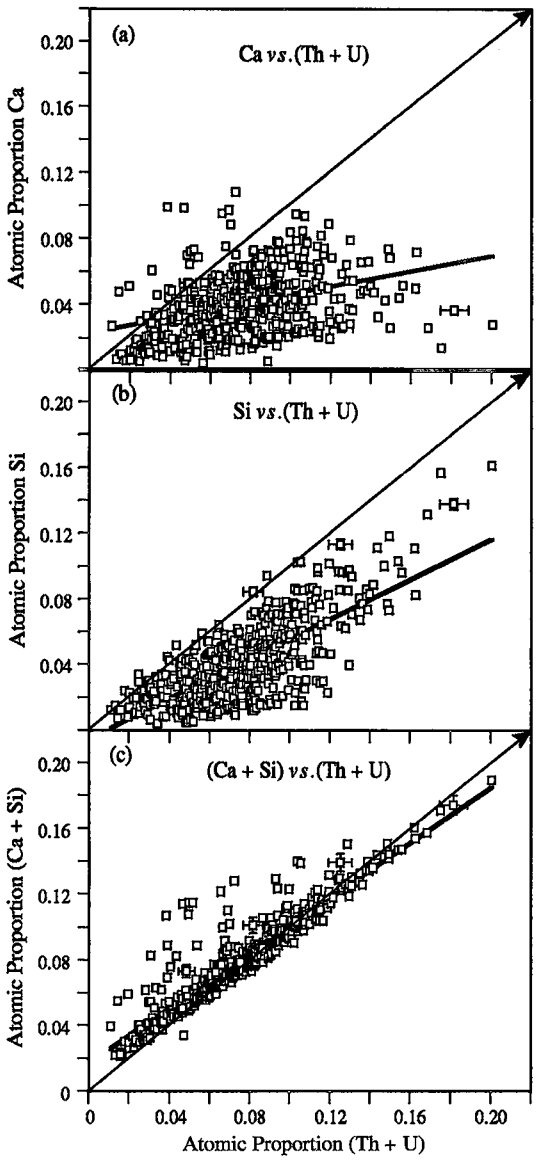

FIG. 1. Plots of the atomic proportion of (a) Ca, (b) Si and (c) Ca + Si against the atomic proportion of Th + U in monazite, based on all single-point determinations of its composition. The line of best fit is shown by the thick lines, whereas the lines with an arrowhead have a slope equal to 1. The error bars represent two standard deviations of the counting statistics.

If schemes (1) and (2) are the only mechanisms of substitution occurring in the monazite grains analyzed, then all data points in Figures 1a – c should fall on or below a line of slope equal to 1 (representing 1:1 actinide to Ca, Si and Ca + Si substitutions, respectively). Clearly, a third mechanism must exist for those grains corresponding to data points in Figure 1a that lie well above the line of slope 1 expected for mechanism 1. The level of excess Ca in these grains (up to 0.069 *apfu*) cannot be held in structural vacancies or defects on account of the strongly ionic nature of the *REE* – oxygen bond in monazite (as indicated by the relatively large difference in electronegativity between the *REE* and oxygen). The combined excess of Ca and Si for these points in Figure 1c is largely due to an excess of Ca, with the incorporation of Si occurring by mechanism (2). It is proposed that the substitution mechanism: $Ca^{2+} + Ce^{4+} = 2REE^{3+}$ also occurs, in addition to mechanisms (1) and (2), in monazite grains containing a large excess of Ca + Si over Th + U. This mechanism seems to fit within the size restrictions of the monazite structure, as $\bar{r}$ for $^{IX}Ca^{2+}$ and $^{IX}Ce^{4+}$ (1.100 Å) is close to the radius of $^{IX}Gd^{3+}$ (1.107 Å). White & Nelen (1987) have used the above substitution to account for EMPA results on a Ca-rich sample of monazite containing only minor amounts of the actinides. The presence of tetravalent cerium may be induced by charge imbalances in the monazite structure, the crystal chemistry having a stabilizing effect on the higher oxidation state. The source of the Ce^{4+} ion in these particular grains may be from the partial oxidation of Ce^{3+} either in the magma or later, once cerium was incorporated within the monazite structure. It was not possible, however, to determine the existence of Ce^{4+} in these grains because of the high level of Ce combined with other *REE*.

A relatively large proportion of the data points in Figure 1c (particularly those compositions low in Th) lie just above the line of slope 1 corresponding to the substitution (Th + U) ↔ (Ca + Si). To investigate this further, those data points outlined above, for which Ca > (Th + U), were removed from the data set, and the remaining data split into two sets on the basis of the combined level of Th and U. These data sets were subjected to statistical analysis and then used to produce the plots shown in Figures 3a – f. A comparison of Figure 3a and 3c suggests that the small excess of Ca + Si over Th + U is due largely to excess Si, as the plot of Si *versus* (Th + U) for low-Th monazite (Fig. 3c) has a significant positive *y*-intercept (Table 3). The amount of combined Ca + Si in excess of the combined level of Th + U decreases for higher levels of Th + U. This is shown by comparison of Figures 3e and 3f. Figure 3f has most data points on or below the line of 1:1 slope, whereas the majority of the points in Figure 3e lie above the 1:1 slope line. This effect may be the

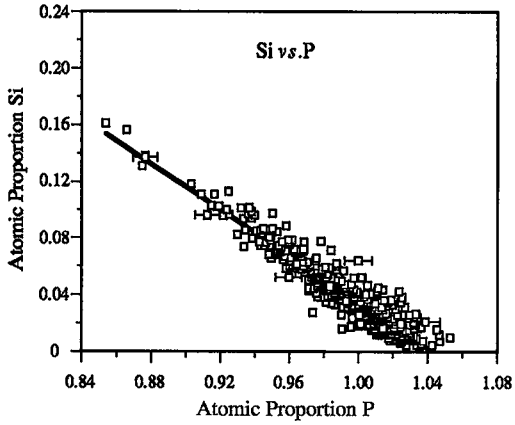

FIG. 2. Plot of the atomic proportion of Si against the atomic proportion of P in monazite, based on all single-point determinations of its composition, showing the line of best fit.

result of a relatively large and somewhat uncertain mass-absorption correction for Si in the presence of heavier atoms in the matrix.

The substitution characteristics of the monazite grains analyzed in this work show a degree of variation from Ca-controlled substitution (mechanism 1) to Si-controlled substitution (mechanism 2), indicated by a variation in the atomic ratio Ca/Si from 10 to 0.1. There is a general increase in the extent of substitution occurring by mechanism (2) for progressively higher levels of Th. This is shown by the difference in the average atomic Ca/Si value (Ca/Si = 1.05) for those grains low in Th (for which the combined atomic proportion of Th and U is less than 0.075), to that for grains high in Th [atomic (Th + U) ≥ 0.075], where Ca/Si is equal to 0.85. The change in substitution behavior described above can be noted from the change in the slope of the lines of best fit (shown as thick lines) for plots of Ca *versus* Th + U, and Si *versus* Th + U for low (Figs. 3a, c) and high (Figs. 3b, d) combined Th and U levels.

TABLE 3. LINEAR REGRESSION ANALYSES FOR SELECTED MODES OF INCORPORATION OF THORIUM AND URANIUM IN MONAZITE

		Correlation Coefficient	Linear regression			
		R	Slope	Std	Intercept	Std
(Ca+Si) *vs.* (Th+U)	1	0.93	0.84	0.01	0.017	0.001
	2	0.69	0.78	0.05	0.020	0.003
	3	0.95	0.92	0.02	0.008	0.002
Ca *vs.* (Th+U)	1	0.36	0.22	0.03	0.023	0.002
	2	0.36	0.43	0.07	0.011	0.004
	3	0.06	0.06	0.05	0.042	0.005
Si *vs.* (Th+U)	1	0.74	0.62	0.05	-0.007	0.002
	2	0.39	0.36	0.03	0.009	0.003
	3	0.73	0.88	0.05	-0.034	0.006
Si *vs.* P	1	0.95	-0.82	0.05	0.853	0.012
	2	0.86	-0.70	0.01	0.729	0.027
	3	0.95	-0.83	0.03	0.869	0.016

Note : Std = Standard deviation.
Grains analysed : 1. All 500 grains analysed.
2. 221 analyses of low thorium grains where the atomic proportion of (Th + U) < 0.075 and Ca < (Th + U).
3. 253 analyses of high thorium grains where the atomic proportion of (Th + U) ≥ 0.075.

Mechanisms of substitution in xenotime

The level of actinide substitution (in particular that of Th) is considerably lower in the xenotime samples than in the monazite samples (*cf.* Tables 1, 2). The level of U in xenotime is, however, generally higher than in the monazite samples analyzed. The presence of significant Si and Ca, in addition to Th and U, indicates that mechanisms of actinide incorporation similar to those found in monazite may also occur in xenotime. The low level of Ca (mean 0.06 wt% oxide), however, suggests that mechanism (1), found to be important in monazite, is not so important in xenotime. A comparison of the slope of the best-fit lines in Figures 4a – c [Ca/(Th + U) slope = +0.08, Si/(Th + U) slope = +0.92 and (Ca + Si)/(Th + U) slope = +1.00] and the corresponding correlation-coefficients shown in Table 4 indicates that mechanism (2) dominates. Incorporation of actinides by mechanism (1) is not favorable owing to the relatively large size of the Ca ion [$r(^{VIII}Ca)$ = 1.120 Å ≈ $r(LREE\ ^{VIII}Pr^{3+})$ = 1.126 Å] in comparison to the *HREE*. The minor amount of incorporation by this mechanism occurs in association with an equivalent amount of U^{4+} and not Th^{4+}. This is indicated by the value of the correlation coefficients of U, Th, and Th + U with Ca for all xenotime compositions containing levels of all substituents above detection limits (Table 4). This behavior can be explained by the difference in the radius of $^{VIII}U^{4+}$ (1.00 Å) and $^{VIII}Th^{4+}$ (1.05 Å). This results in the values of $\bar{r}$ equal to 1.060 Å and 1.085 Å for the combinations Ca^{2+} and U^{4+}, and Ca^{2+} and Th^{4+}

TABLE 4. CORRELATION MATRIX FOR SELECTED MODES OF INCORPORATION OF THORIUM AND URANIUM IN XENOTIME*

Element	Th	U	Th+U	Ca	Si	Ca+Si	P
Th	1	0.07	0.58	-0.14	0.69	0.63	-0.51
U	0.07	1	0.85	0.49	0.62	0.70	-0.63
Th+U	0.58	0.85	1	0.32	0.87	0.90	-0.77
Ca	-0.14	0.49	0.32	1	0.09	0.30	-0.10
Si	0.69	0.62	0.87	0.09	1	0.98	-0.74
Ca+Si	0.63	0.70	0.90	0.30	0.98	1	-0.74
P	-0.51	-0.63	-0.77	-0.10	-0.74	-0.74	1

Note : With 126 analyses used a correlation coefficent of 0.19 is significant at the 5% level.
* Only those grains analysed containing above detection limit levels of all substituents are included.

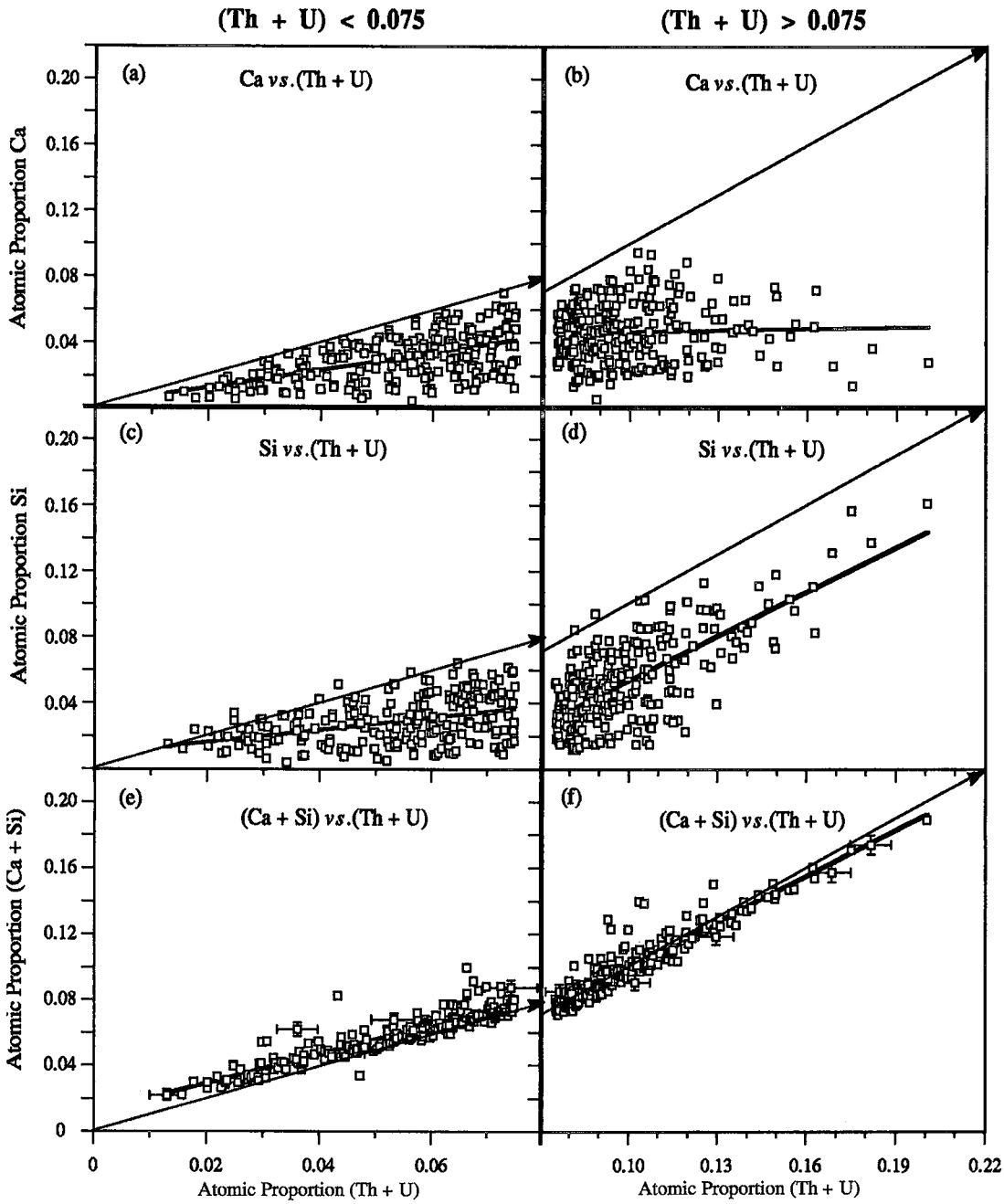

FIG. 3. Plots of the atomic proportion of Ca (a) and (b), Si (c) and (d), and Ca + Si (e) and (f) against the atomic proportion of Th + U for monazite grains either poor (Th + U < 0.075 *apfu*) (a, c, e) or rich (Th + U ≥ 0.075 *apfu*) (b, d, f) in Th. Points for which Ca > (Th + U) have been excluded. The line of best fit is shown by the thick lines, whereas the lines with an arrowhead have a slope equal to 1. Note: there is a change in the *x*-axis scale from (a), (c) and (e) to (b), (d) and (f).

respectively. Since the value of $\bar{r}$ of Ca^{2+} and U^{4+} is close to the radius of $^{VIII}Gd^{3+}$ (1.053 Å), and since Gd^{3+} is found in appreciable amounts in xenotime samples (Table 2), substitution of Ca with U is possible (on the basis of $\bar{r}$ arguments) in this mineral. As the $\bar{r}$ of Ca^{2+} and Th^{4+} ($\approx \bar{r}$ of $^{VIII}Sm^{3+}$ = 1.079 Å) is considerably larger than that of Ca^{2+} and U^{4+}, the incorporation of Ca with Th occurs only in the monazite structure.

The incorporation of Th and U *via* mechanism (2) was expected, since both $USiO_4$ and $ThSiO_4$ (mineral name: thorite) can exist in the zircon structure-type adopted by xenotime (Fuchs & Gebert 1958). Indeed, a complete solid-solution (in the zircon structure-type) seems to exist between $USiO_4$ and $ThSiO_4$ (Fuchs & Gebert 1958). Further evidence that U can be incorporated in xenotime by both mechanisms (1) and (2) is found in the study of the composition of U-rich xenotime by Parnell (1989), who has found several samples with large amounts of both Ca and Si (but no Th) in addition to U.

The negative correlation (R = -0.78) between the atomic proportions of P and Si shown in Figure 5 provides further evidence of the existence of mechanism (2) in xenotime. The slope of the line of best fit in Figure 5, Si/P = -0.93, is close to that expected for the 1:1 replacement of P with Si occurring *via* mechanism (2). No mention has been made previously of the relationship between P and Si in xenotime.

If only substitution mechanisms (1) and (2) occur in the xenotime grains analyzed, then all the points in Figure 4a – c should lie on or below the line of slope 1. Examination of Figure 4b shows that most xenotime compositions lie above the line representing a slope of Si/(Th + U) equal to 1. An additional mechanism involving the incorporation of Si and not Th or U must be present [in addition to mechanisms (1) and (2)] in most of the xenotime grains analyzed to account for the level of Si (too high by 0.007 *apfu*). The possibility of the excess Si entering together with an OH species *via*

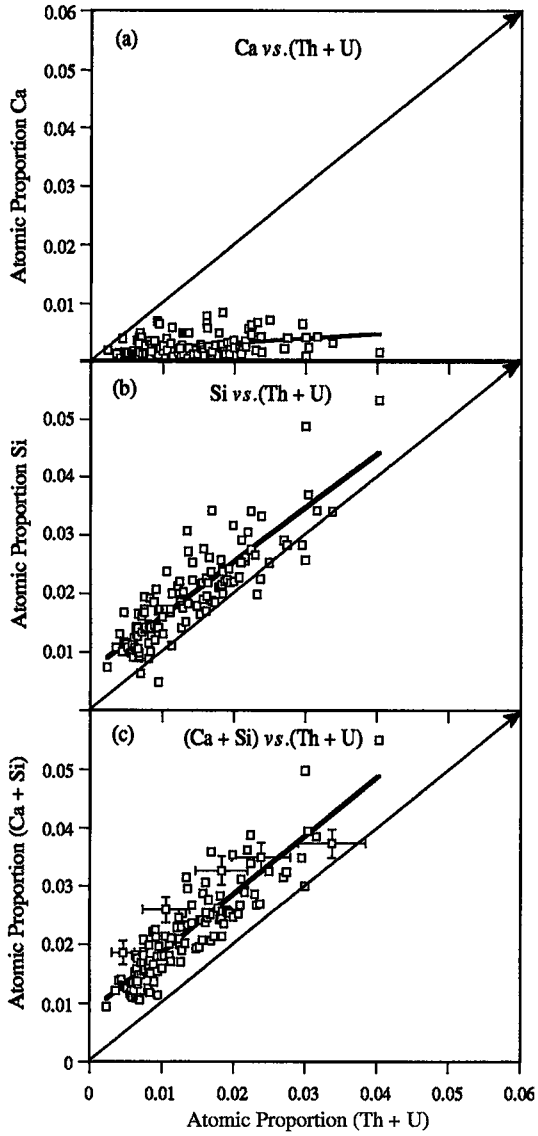

FIG. 4. Plots of the atomic proportion of Ca (a), Si (b), and Ca + Si (c) against the atomic proportion of Th + U in xenotime, based on single-point determinations of its composition for which the level of the elements plotted is greater than the detection limit. The line of best fit is shown by the thick lines, whereas the lines with an arrowhead have a slope equal to 1.

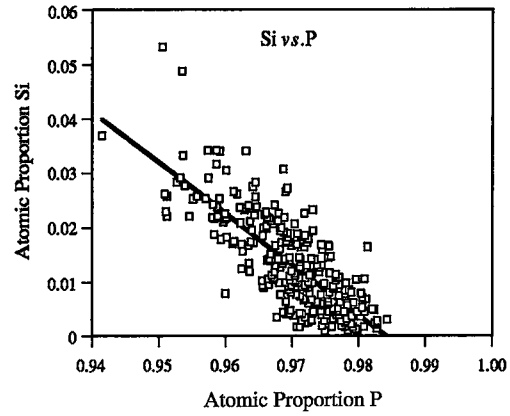

FIG. 5. Plot of the atomic proportion of Si against the atomic proportion of P in xenotime, based on all single-point determinations of its composition for which the level of Si is greater than the detection limit.

the mechanism : $Si^{4+} + OH^- = P^{5+} + O^{2-}$ was investigated by looking for the presence of the OH vibration frequencies in the infrared reflectance spectra of a number of individual grains of xenotime. The presence of OH in xenotime was considered, as it has been found in the isostructural minerals zircon and thorite (together with molecular water) (Lumpkin & Chakoumakos 1988). No evidence was found to suggest the presence of OH from the infrared spectra of several grains examined. It is difficult to rationalize how this excess Si is accommodated in the zircon structure-type, as no Ce (and hence no Ce^{4+}) was detected in the WDS spectral scans. A small amount of Ce or Tb in the tetravalent state, or a minor proportion of U in the pentavalent state, in combination with the excess Si cannot, however, be ruled out.

Conclusions

Consideration of size restrictions such as the $\bar{r}$ of the *REE* site in the monazite and xenotime structures can be used to explain the actinide substitution in each mineral. Th and U substitution in each structure occurs *via* a combination of the two charge-balance-maintaining mechanisms : $(Th, U)^{4+} + Ca^{2+} = 2REE^{3+}$ and $(Th,U)^{4+} + Si^{4+} = REE^{3+} + P^{5+}$. Actinide incorporation in monazite is dominated by Th, and can be described by an approximately equal contribution of both mechanisms. Although the level of actinides in xenotime is significantly lower than that found in monazite, their incorporation into the zircon structure-type of xenotime can also be explained by the same two mechanisms. However, owing to the more rigid size-constraints imposed by the zircon structure, the first of these mechanisms is of only minor importance.

Mechanisms in addition to those above must exist in both monazite and xenotime minerals to account for combined levels of the substituents Ca and Si that exceed those of the actinides Th and U. Levels of Ca in monazite can perhaps be explained by an equivalent amount of Ce^{4+}.

Acknowledgements

Special thanks are extended to Mr. B.W. Robinson and Dr. G.J. Hitchen for assistance in the use of the electron-microprobe facilities at CSIRO. Dr. N.G. Ware of the Australian National University is thanked for the loan of the *REE* oxy-phosphate standards used in the determination of peak-overlap corrections. Drs. T.C. Parks and E.H. Nickel are thanked for useful discussions concerning the content of the paper. One of us (BVE) thanks the Australian government for an Australian Postgraduate Award, and the Research Centre for Advanced Mineral and Materials Processing for supplementary funds. The comments of the reviewers and the editor greatly improved the presentation of our findings.

References

Åmli, R. (1975): Mineralogy and rare earth geochemistry of apatite and xenotime from the Gloserheia granite pegmatite, Froland, southern Norway. *Am. Mineral.* **60**, 607-620.

Baxter, J.L. (1990): Heavy mineral sand deposits of Western Australia. *In* Geology of the Mineral Deposits of Australia and Papua New Guinea (F.E. Hughes, ed.). The Australian Institute of Mining and Metallurgy, Melbourne, Australia.

Boatner, L.A. & Sales, B.C. (1988): Monazite. *In* Radioactive Waste Forms for the Future (W. Lutze & R.C. Ewing, eds.). Elsevier Science, Amsterdam, The Netherlands (495-564).

Casillas, R., Nagy, G., Pantó, G., Brändle, J. & Fórizs, I. (1995): Occurrence of Th, U, Y, Zr, and REE-bearing accessory minerals in late-Variscan granitic rocks from the Sierra de Guadarrama (Spain). *Eur. J. Mineral.* **7**, 989-1006.

Colby, T.W. (1968): *MAGIC Computer Program for Quantitative Electron Microprobe Analysis.* Bell Telephone Laboratories, Allentown, Pennsylvania.

Demartin, F., Pilati, T., Diella, V., Donzelli, S., Gentile, P. & Gramaccioli, C.M. (1991a): The chemical composition of xenotime from fissures and pegmatites in the Alps. *Can. Mineral.* **29**, 69-75.

———, ———, ———, ——— & Gramaccioli, C.M. (1991b): Alpine monazite: further data. *Can. Mineral.* **29**, 61-67.

Drake, M.J. & Weill, D.F. (1972): New rare earth element standards for electron microprobe analysis. *Chem. Geol.* **10**, 179-181.

Fuchs, L.H. & Gebert, E. (1958): X-ray studies of synthetic coffinite, thorite and uranothorites. *Am. Mineral.* **43**, 243-248.

Gramaccioli, C.M. & Segalstad, T.V. (1978): A U- and Th-rich monazite from a south-alpine pegmatite at Piona, Italy. *Am. Mineral.* **63**, 757-761.

Jefferies, N.L. (1985): The distribution of the rare earth elements within the Carnmenellis pluton, Cornwall. *Mineral. Mag.* **49**, 495-504.

Jefford, G. (1962): Xenotime from Rayfield, northern Nigeria. *Am. Mineral.* **47**, 1467-1473.

Kamineni, D.C., Rao, A.T. & Bonardi, M. (1991): The geochemistry of monazite types from the eastern Ghats granulite terrain, India. *Mineral. Petrol.* **45**, 119-130.

Lumpkin, G.R. & Chakoumakos, B.C. (1988): Chemistry and radiation effects of thorite-group minerals from the Harding pegmatite, Taos County, New Mexico. *Am. Mineral.* **73**, 1405-1419.

Mannucci, G., Diella, V., Gramaccioli, C.M. & Pilati, T. (1986): A comparative study of some pegmatitic and fissure monazite from the Alps. *Can. Mineral.* **24**, 469-474.

McCarthy, G.J., White, W.B. & Pfoertsch, D.E. (1978): Synthesis of nuclear waste monazites, ideal actinide hosts for geologic disposal. *Mater. Res. Bull.* **13**, 1239-1245.

Montel, J.-M. (1993): A model for monazite/melt equilibrium and application to the generation of granitic magmas. *Chem. Geol.* **110**, 127-146.

Murata, K.J., Dutra, C.V., Teixeira Da Costa, M. & Branco, J.J.R. (1958): Composition of monazites from pegmatites in eastern Minas Gerais, Brazil. *Geochim. Cosmochim. Acta* **16**, 1-14.

Muto, T., Meyrowitz, R., Pommer, A.M. & Murano, T. (1959): Ningyoite, a new uranous phosphate mineral from Japan. *Am. Mineral.* **44**, 633-650.

Ni, Yunxiang, Hughes, J.M. & Mariano, A.N. (1995): Crystal chemistry of the monazite and xenotime structures. *Am. Mineral.* **80**, 21-26.

Parnell, J. (1989): Uranium-rich xenotime in bitumen, Moonta mines, South Australia. *Aust. Mineral.* **4**, 145-148.

Petersen, O.V. & Gault, R.A. (1993): Xenotime from the Narssârssuk pegmatite, South Greenland. *Neues Jahrb. Mineral., Monatsh.*, 259-264.

Roeder, P.L. (1985): Electron-microprobe analysis of minerals for rare-earth elements: use of calculated peak-overlap corrections. *Can. Mineral.* **23**, 263-271.

Rose, D. (1980): Brabantite, $CaTh[PO_4]_2$, a new mineral of the monazite group. *Neues Jahrb. Mineral., Monatsh.* 247-257.

Satterthwaite, K. (1994): Rare Earths. *In* Metals and Minerals Annual Review – 1994. Mining Journal Limited, London, U.K. (72-74).

Shannon, R.D. (1976): Revised effective ionic radii and systematic studies of interatomic distances in halides and chalcogenides. *Acta Crystallogr.* **A32**, 751-767.

Taylor, M. & Ewing, R.C. (1978): The crystal structures of the $ThSiO_4$ polymorphs: huttonite and thorite. *Acta Crystallogr.* **B34**, 1074-1079.

Wark, D.A. & Miller, C.F. (1993): Accessory mineral behavior during differentiation of a granite suite: monazite, xenotime and zircon in the Sweetwater Wash pluton, southeastern California, U.S.A. *Chem. Geol.* **110**, 49-67.

White, J.S. & Nelen, J.E. (1987): Monazite and calcioancylite from the Foote mine, North Carolina. *Mineral. Rec.* **18**, 203-205.

Received February 26, 1996, revised manuscript accepted August 29, 1996.